

How Does Reasoning Flow? Tracing Attention-Induced Information Flow for Targeted RL in LLMs

Zhichen Dong^{*123} Yang Li^{*12} Yuhan Sun¹ Weixun Wang² Yijia Luo² Zinian Peng¹
 Taiheng Ye¹ Chao Yang³ Wenbo Su^{†2} YuCheng² Bo Zheng² Junchi Yan^{†1}

¹Shanghai Jiao Tong University ²Alibaba Group ³Shanghai Artificial Intelligence Laboratory

Abstract

Token-level credit assignment remains a key obstacle for reinforcement learning (RL) in large language models (LLMs), where RL recipes typically treat all tokens equally, failing to distinguish decisive reasoning steps from routine formatting or fluent filler. Recent attempts leverage model-internal signals to assign finer-grained credit, but these are often point-wise heuristics that ignore the global structure of information propagation. We propose FlowTracer, an RL framework that traces *answer-targeted reasoning flow* on an attention-induced directed acyclic graph in which nodes correspond to tokens and edge capacities come from aggregated attention weights and derives token credit from this global structure. The edge capacities are reweighted to retain only the influence that can reach the answer region, while enforcing local flow conservation so intermediate tokens neither lose nor gain effective mass due to path length or irrelevant branches. On this graph, FlowTracer extracts an information-flow backbone connecting the question to the answer and scores tokens by flow throughput, revealing high-impact hubs and aggregation checkpoints that mediate long-range dependencies. These derived importances are used to shape token-level rewards, enabling learning signals to focus precisely on the tokens that route information toward (or away from) correct answers and delivering consistent performance gains across a range of reasoning tasks.

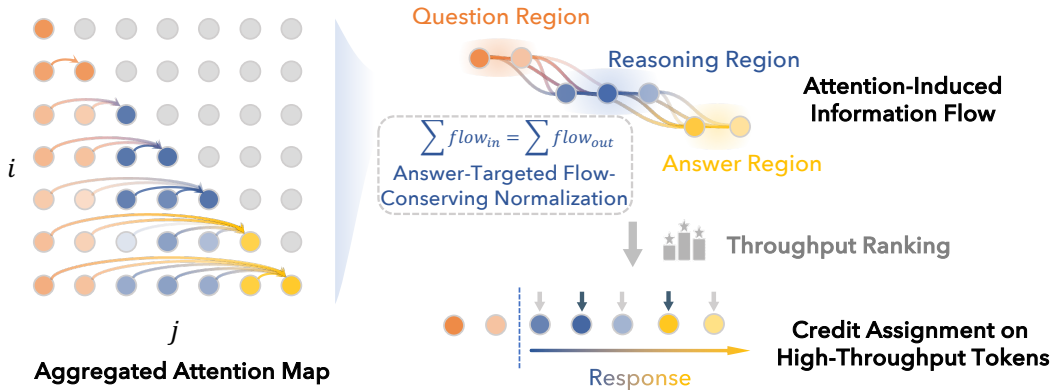


Figure 1: **Overview of FlowTracer.** We build an attention-induced token graph, condition it on the answer to retain only routes that support the prediction, and normalize it to ensure locally consistent flow. Injecting flow from a super-source over the prompt to a super-sink over the answer yields a backbone of dominant multi-hop information paths. Token throughput on this backbone identifies key routing hubs for token-level credit assignment and reward shaping.

1 Introduction

Reinforcement learning (RL) has become an important tool for training and aligning large language models (LLMs), and it has shown particular promise in eliciting and strengthening step-by-step reasoning for complex tasks (Christiano et al., 2017; Jaech et al., 2024; Guo et al., 2025; Team et al., 2025b). Among RL approaches, reinforcement learning with verifiable rewards (RLVR) offers a practical and scalable recipe when automatic checkers are available, providing reliable training signals from deterministic evaluators (Shao et al., 2024; Lambert et al., 2024). This paradigm has driven substantial progress in mathematical problem solving (Xin et al., 2025; Wang et al., 2024; Long et al., 2025), code generation (Hui et al., 2024; Yang et al., 2025a), and more recently agentic settings (Yang et al., 2024; Team et al., 2025a;

^{*}Equal contribution.

[†]Correspondence to: Junchi Yan yanjunchi@sjtu.edu.cn; Wenbo Su vincent.swb@alibaba-inc.com.

Wang et al., 2025d), where sequences of intermediate decisions unfold over long horizons and task success is precisely defined and automatically verifiable.

Despite these gains, a persistent limitation of RL for LLMs is token-level credit assignment. Autoregressive generation produces long trajectories with sparse, delayed supervision (e.g., correctness judged only at the end), so attributing success or failure to individual tokens is inherently challenging. While classical RL tools such as generalized advantage estimation (GAE) (Schulman et al., 2015) can in principle yield token-wise learning signals, they rely on accurate state-value estimates. In practice, estimating token-level value from the outside, i.e., based only on observed text states, is difficult in rich linguistic contexts, which makes attribution noisy and unstable. This often pushes methods toward coarse approximation designs that effectively weight tokens uniformly (Shao et al., 2024; Zheng et al., 2025), obscuring the difference between pivotal reasoning steps and incidental wording. On the other hand, recent works show that the model’s own internal dynamics could provide additional reference signals for credit assignment (Wang et al., 2025b; Cui et al., 2025; Li et al., 2025d), e.g., indicators of when information is being accumulated versus when the model is uncertain or confused. However, existing approaches typically operationalize such cues via point-wise heuristics (e.g., entropy (Wang et al., 2025b;a), attention statistics (Bogdan et al., 2025; Li et al., 2025d)) and largely overlook the global structure of how information propagates and is transformed across the full sequence.

We argue that resolving token-level credit assignment requires answering a more fundamental question: *How does reasoning flow from the prompt to the final answer inside an LLM?* Rather than scoring tokens in isolation, we seek a structured, system-level characterization of how information is routed through intermediate tokens and long-range dependencies. Attention provides an explicit interaction graph among tokens, but raw attention weights alone do not directly reveal which multi-hop routes constitute the dominant backbone that carries task-relevant information. This motivates a graph-theoretic approach that can extract globally consistent paths and identify the true transit hubs that mediate prompt-to-answer transmission.

To this end, we propose FlowTracer, a graph-based credit assignment method that extracts an *answer-targeted reasoning backbone* from the model’s attention structure and uses it to guide RL updates. We view the token sequence as an attention-induced directed acyclic graph (DAG), where each node is a token and each directed edge carries a nonnegative capacity derived from aggregated attention weights, interpreted as the strength of potential information transfer. Our goal is to quantify, for each token, how much of its influence is actually routed toward the answer region, rather than merely being locally salient.

A direct use of raw attention is insufficient for this purpose. Attention graphs contain numerous branches that never contribute to the final answer, and naive propagation on such graphs causes influence to be diluted along long paths or absorbed by irrelevant subtrees. As a result, early but decisive premises can be systematically under-credited, while late-stage tokens near the answer may receive disproportionate weight simply due to proximity. To avoid these structural biases, FlowTracer introduces an explicit *answer-conditioning* step on the attention graph: we first define an answer region (e.g., the final answer span) and compute a global reachability potential that measures how much downstream influence from each token can ultimately reach the answer. We then *reweight* outgoing edge capacities to keep only the answer-relevant portion of influence and to satisfy a local flow-conservation property, ensuring that intermediate tokens neither lose nor gain effective mass due to path length, fan-out, or irrelevant branches. Tokens with zero answer-reachability are naturally filtered out, yielding a cleaned, target-conditioned graph that focuses analysis on the effective reasoning substructure.

On this target-conditioned graph, FlowTracer performs a flow analysis between the prompt and the answer. By injecting unit flow from a super-source connected to prompt tokens and collecting flow at a super-sink connected to answer tokens, we recover an information-flow backbone that highlights the dominant multi-hop routes supporting the final prediction. The resulting token throughputs discover the reasoning pattern where high-throughput tokens act as transit hubs or aggregation checkpoints that mediate long-range dependencies (e.g., periodic consolidation near clause boundaries, repeated symbols, or variables that serve as cross-step anchors). By applying the resulting token throughputs, we plug the globally consistent notion of credits into RLVR via token-level reward shaping and loss reweighting, amplifying learning signals on high-impact routing tokens and suppressing updates on low-impact filler, thereby improving both learning efficiency and reasoning performance.

2 Related Work

Deriving Optimization Signals From LLM Internal Dynamics. Generative modeling has shown promise in broad scenarios (Li et al., 2026; 2025e; Chen et al., 2026; Wang et al., 2026). While traditional optimization treats LLMs as black-box generators for end-to-end optimization, recent studies exploit internal computational processes to extract fine-grained signals (Zou et al., 2023; Chen et al., 2024; Dong et al.,

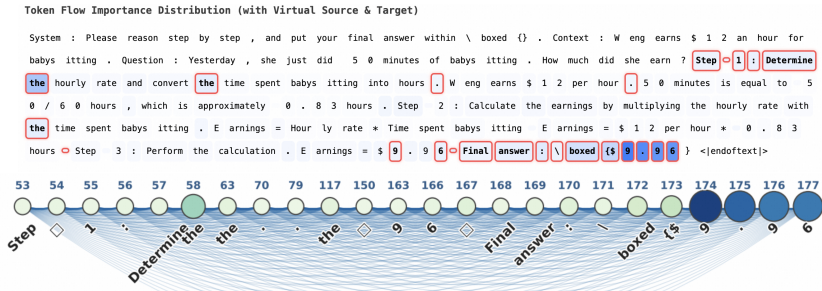


Figure 2: Answer-targeted token flow importance in Qwen3-4B. By modeling the generation as a DAG, we trace the influence flow from the prompt to the final answer. Darker nodes indicate higher flow throughput, identifying a reasoning backbone of decisive tokens over routine filler. This enables finer-grained token-level credit assignment for targeted RL.



Figure 3: Word cloud of high-flow and low-flow tokens.

2025). Research identifies specific components crucial for information handling, including task-specific attention heads (Cabannes et al., 2024; Bertolazzi et al., 2025), context-aggregating receiver heads (Ren et al., 2024; Zheng et al., 2024), specialized functional layers (Dumitru et al., 2024), and steering directions in representation space (Burns et al., 2022; Venhoff et al., 2025). These insights enable LLM augmentation via representation editing (Hernandez et al., 2023; Turner et al., 2023), side-route classifiers (Li et al., 2022; Belrose et al., 2023; Ji et al., 2024), and component-focused training (Zhao et al., 2025). Beyond static analysis, dynamic methods examine information propagation via attention (Geva et al., 2023; Bogdan et al., 2025). This reveals internal traits such as factual association (Geva et al., 2023; Mohebbi et al., 2023), multi-path calculation (Dutta et al., 2024; Ameisen et al., 2025) and critical reasoning steps (Bogdan et al., 2025; Minegishi et al., 2025; Qian et al., 2025). However, raw attention is noisy and limited to single-step, point-wise influence. To this end, we apply a Doob-h-like transform to isolate the answer-relevant multi-hop reasoning backbone, yielding a robust signal to guide optimization. This view is also related to recent label-repurposing ideas, in which ground-truth labels are treated not merely as loss targets but as informative references that guide prediction learning (Li et al., 2025f).

Credit Assignment for RL in LLMs. RL is standard for LLM post-training (Ziegler et al., 2019; Ouyang et al., 2022; Achiam et al., 2023; Lu et al., 2025), yet effective credit assignment remains an evolving challenge (Lin et al., 2024; Vassoyan et al., 2025; Liu et al., 2026; Dong et al., 2024). Off-policy RL (Rafailov et al., 2023; Meng et al., 2024) aligns probabilities, while more prevailing on-policy RL relies on sparse outcome rewards (Bai et al., 2022). Explicit step-wise supervision (e.g., PRMs (Lightman et al., 2023) or MCTS (Guan et al., 2025)) mitigates sparsity but faces reward hacking and efficiency bottlenecks (Cheng et al., 2025b). With the emergence of RLVR (Shao et al., 2024; Lambert et al., 2024), Group Relative Policy Optimization (GRPO) (Xin et al., 2025) bypasses these limitations by using group advantage as an implicit signal to induce reasoning behaviors (Yu et al., 2025; Yang et al., 2025a). Yet, this approach distributes credit uniformly, failing to distinguish critical steps from fillers (Gandhi et al., 2025; Li et al., 2025a). Recent works improve this with signals like entropy (Wang et al., 2025b;a; Cheng et al., 2025a; Cui et al., 2025), confidence or correlation (Li et al., 2025c; Zhou et al., 2024b; Nie et al., 2025; Zhou et al., 2024a), gradients (Green et al., 2025; Li et al., 2025b) and attention (Li et al., 2025d), but these remain point-wise and ignore inter-token relationships. Our method models multi-hop influence within the reasoning flow to identify a token’s true contribution, yielding a more precise credit assignment.

3 Methodology

We present FlowTracer, a principled framework for token-level credit assignment in reinforcement learning (RL) for large language models (LLMs). Our approach leverages the global structure of attention-induced information propagation to identify which tokens genuinely contribute to the final answer. The method rests on three core ideas: (1) modeling reasoning as influence flow over a directed acyclic graph (DAG) induced by attention; (2) enforcing answer-targeted flow conservation through a Doob-h-like reweighting, followed by forward propagation to compute token-level throughput; and (3) using the resulting flow throughput to drive fine-grained, non-uniform policy updates. Crucially, we interpret attention weights as non-negative *influence couplings* and exploit their algebraic structure to isolate only those paths that meaningfully contribute to the final output.

3.1 Answer-Targeted Influence Flow on Attention-Induced DAGs

We formalize reasoning as a linear influence propagation process over an attention-induced directed acyclic graph (DAG), and compute a conserved flow that isolates influence paths that ultimately reach the answer. This consists of three stages: (1) constructing a raw influence graph from attention, (2) reweighting edges via a Doob-h-like transform to enforce answer-targeted conservation, and (3) propagating unit source flow forward to obtain token-level credit.

Raw Influence Graph from Attention. Given an input-output sequence (x_1, \dots, x_T) generated by an LLM, we construct a time-ordered DAG $\mathcal{G} = (V, E)$ where each token x_i corresponds to a node $v_i \in V$, and a directed edge $E_{i \rightarrow k}$ exists for all $i < k$. The edge weight $W_{ik} \geq 0$ is derived from aggregated attention scores (e.g., mean over attention layers and heads) $a(x_k, x_i)$:

$$W_{ik} := a(x_k, x_i) \geq 0, \quad (1)$$

We interpret W_{ik} as the *local influence coupling strength*: when one unit of influence departs from x_i , a fraction W_{ik} is absorbed by x_k and may be further propagated. Critically, we do not require $\sum_{k>i} W_{ik} = 1$; thus, the out-degree sum may exceed 1 (parallel broadcasting) or fall below 1 (signal attenuation), and W defines a linear operator instead of a stochastic kernel.

While attention weights provide a natural signal for inter-token dependencies, using the raw attention graph W directly for credit propagation suffers from two critical issues that undermine structured reasoning analysis: First, **attention violates local flow conservation**. Standard attention weights are normalized over *source tokens* for each target, i.e., $\sum_{i<k} W_{ik} = 1$ (in-degree normalization). However, the out-degree sum $\sum_{k>i} W_{ik}$ is generally *not equal to 1*; it can be arbitrarily large (if x_i attends broadly) or small (if x_i is ignored). Consequently, when influence flows forward from a node, it may be amplified or attenuated purely due to graph topology, not semantic importance. Second, and more fundamentally, **the raw graph contains extensive answer-irrelevant substructures**. A large fraction of attention flows into filler tokens, formatting markers, or intermediate hypotheses that are later discarded, i.e., paths that terminate before contributing to the final answer. Propagating credit through such dead-end branches leads to systematic underestimation of early critical premises (due to exponential decay over spurious paths) and overemphasis on tokens near the answer that merely restate conclusions.

Doob-h-Like Reweighting for Effective Influence. To resolve both issues, we seek a reweighted graph W' that (1) enforces *local flow conservation* ($\sum_{k>i} W'_{ik} = 1$) and (2) restricts propagation to only those paths that ultimately reach the answer. We achieve this via a *Doob-h-like reweighting*, where $h(i)$ denotes the total influence from node i that successfully reaches the answer. We introduce a virtual sink node s connected from all answer tokens \mathcal{A} and then define a potential function $h(i)$ indicating the *effective reachability* to the answer as the total influence-weighted path sum from node i to s :

$$h(s) = 1, \quad h(i) = \sum_{k>i} W_{ik} h(k), \quad \forall i \notin \mathcal{A}. \quad (2)$$

Then we set

$$W'_{ik} := \frac{W_{ik} h(k)}{h(i)}. \quad (3)$$

This transformation guarantees a critical structural property:

Theorem 3.1 (Local Flow Conservation). *For any node i with $h(i) > 0$, the reweighted outflow sums to unity:*

$$\sum_{k>i} W'_{ik} = 1.$$

Proof. By definition of $h(i)$ in Eq. 2, $\sum_{k>i} W'_{ik} = \sum_{k>i} \frac{W_{ik} h(k)}{h(i)} = \frac{1}{h(i)} \sum_{k>i} W_{ik} h(k) = \frac{h(i)}{h(i)} = 1$. \square

Theorem 3.1 ensures that effective influence is neither created nor destroyed at intermediate nodes, eliminating bias from graph topology. Simultaneously, by scaling edges with $h(k)/h(i)$, the reweighting automatically suppresses flow into dead-end branches (where $h(k) \approx 0$) and reallocates it to answer-reaching paths. Consequently, W'_{ik} represents the *fraction of node i 's total answer-reaching influence that is routed through successor k* , yielding a conserved, answer-targeted flow field suitable for structured credit assignment.

Table 1: Causal intervention results on GSM8K. We perturb 20% of tokens based on different selection methods and measure their impact on reasoning outcomes.

Perturbation Target	Answer Change \uparrow	Correctness Reverse \uparrow
Random (20%)	29.5%	4.5%
Low-flow (Bottom 20%)	14.9%	0.5%
High-flow (Top 20%)	45.9%	14.9%

Forward Flow for Token-Level Throughput. To obtain a token-level estimate of credit, we inject a unit of influence from the question and compute the resulting flow through the answer-targeted DAG. Specifically, we introduce a virtual source node \mathcal{S} connected to all input (question) tokens \mathcal{Q} with initial flow $f(\mathcal{S} \rightarrow i) = 1/|\mathcal{Q}|$. We then propagate this influence forward over the reweighted, flow-conserving graph W' :

$$f(k) = \sum_{i < k} f(i) W'_{ik}, \quad \forall k. \quad (4)$$

The resulting $f(k)$ represents the *share of effective influence* originating from the question and destined for the answer that passes through token x_k . The edge flow $\phi(i \rightarrow k) = f(i)W'_{ik}$ measures the importance of the dependency $x_i \rightarrow x_k$ in the reasoning backbone. Tokens with high total throughput $\tau(k) = f(k) + \sum_{j > k} \phi(k \rightarrow j)$ are identified as nodes that play a critical role in shaping the final answer. Consequently, we expect reinforcement learning signals to be most effectively propagated through these hubs, making them natural targets for fine-grained credit assignment and policy optimization.

3.2 High-Flow Tokens as the Backbone of Reasoning

In this section, building on the formalized answer-targeted influence flow, we analyze the information flow within LLM reasoning. We conduct analytical experiments using the Qwen3-4B-Base (Yang et al., 2025a) model on the GSM8K (Cobbe et al., 2021) math reasoning dataset. Specifically, we (1) identify flow patterns characterized by high-flow information hubs (i.e. high-flow tokens) and (2) causally demonstrate their influence on the final answer. These findings support the use of high-flow tokens as fine-grained signals for policy optimization credit assignment.

High-flow information hubs appear as periodic bridges to form the reasoning backbone. Our analysis reveals that information flow is not uniformly distributed; instead, it exhibits a “backbone” structure where sparse, high-flow hubs emerge periodically. As illustrated in Fig. 3, tokens with high throughput $\tau(k)$ typically act as *structural delimiters* (e.g., punctuation, newlines) or *symbolic anchors* (e.g., recurrent variable names, mathematical operators). As exemplified in Fig. 2, these tokens appear periodically to aggregate the context and broadcast it to future tokens, governing the local information flow until it is re-consolidated by another high-flow hub. Conversely, low-flow tokens generally consist of semantic filler, such as nouns and verbs, that support the sentence structure rather than the logical progression. This separation suggests that the model naturally decouples “generating logic” (high-flow) from “maintaining fluency” (low-flow).

Causal intervention validates: high-flow tokens act as backbones of reasoning, as blocking information aggregated at these points strongly influences the final answer. To verify that high-flow hubs are causal drivers of reasoning, we conduct an intervention experiment on the GSM8K dataset. We identify high-flow and low-flow tokens, then perform perturbations by masking the attention of 20% of the tokens (comparing high-flow, low-flow, and random selections) to prevent information from passing forward during regeneration. We measure the effect using the *answer change rate* (e.g. 17 \rightarrow 37) and *correctness reverse rate* (e.g., correct \rightarrow wrong). The results in Table 1 show a distinct divergence: **perturbing high-flow tokens leads to sharp answer changes and significant correctness shifts, whereas perturbing low-flow or random tokens alters the outcome minimally.** This confirms that high-flow tokens serve as delegates for critical information hubs; therefore, high-flow tokens act as key pivot points for the reasoning process, providing natural model-internal signals for fine-grained optimization.

3.3 Credit Assignment via High-Flow Tokens

Based on the findings above, we augment RL training via **fine-grained credit assignment** using the derived high-flow token backbone. Specifically, traditional RL methods for LLMs typically assign a uniform reward to every token, implicitly assuming equal contribution to the final answer. We challenge this by assigning higher credit to the specific tokens that drive the final output. This attributes the outcome

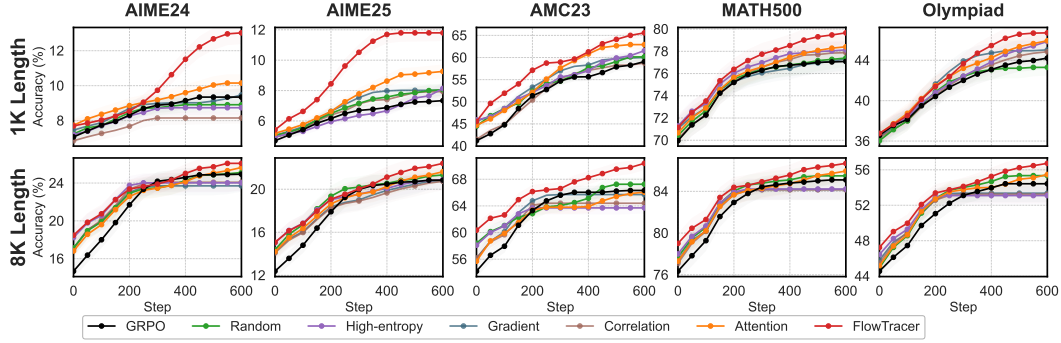


Figure 4: Performance curves of RL training on math reasoning based on the Qwen3-8B-Base model, with 1K and 8K length respectively.

(e.g., correct or incorrect) to the true driver tokens, enabling more efficient and accurate training. Below, we detail (1) our efficient implementation within RL frameworks and (2) our credit assignment strategy.

Efficient Integration into RL Frameworks. Credit assignment occurs between the sampling and training stages. To compute flow for the generated responses within the RL loop, we perform a single additional forward pass to extract attention maps from middle layers (averaging layers $L/3 \sim 2L/3$). We then apply our answer-targeted flow computation (Section 3.1) to identify the top 40% high-flow tokens, which are used to weight policy updates. **Notably, this introduces only a marginal time overhead of 2.2%–4.5% (detailed in Sec. 4.3)**, as the cost of a single forward pass is negligible compared to the thousands of autoregressive generation steps of sampling, leaving the time-consuming training stage. The specific layers and top- k ratios are selected empirically (also demonstrated in Sec. 4.3), with full implementation details provided in Section C.

Credit Assignment in RL. To assign distinct credit (and consequently varying reward or loss) to each token based on its contribution to the final answer, we introduce a non-uniform scaling factor $\gamma_{i,t}$ into the GRPO loss:

$$\mathcal{J}(\theta) = \mathbb{E}_{\mathbf{x} \sim \mathcal{D}} \left[\frac{1}{G} \sum_{i=1}^G \frac{1}{N_i} \sum_{t=1}^{N_i} \gamma_{i,t} \cdot \min \left(\frac{\pi_{\theta}(y_{i,t} | \mathbf{x}, \mathbf{y}_{i,<t})}{\pi_{\theta_{\text{old}}}(y_{i,t} | \mathbf{x}, \mathbf{y}_{i,<t})} \hat{A}_i, \text{clip} \left(\frac{\pi_{\theta}(y_{i,t} | \mathbf{x}, \mathbf{y}_{i,<t})}{\pi_{\theta_{\text{old}}}(y_{i,t} | \mathbf{x}, \mathbf{y}_{i,<t})}, 1 - \epsilon, 1 + \epsilon \right) \hat{A}_i \right) \right] \quad (5)$$

In standard GRPO, $\gamma_{i,t}$ is typically set to 1 or acts as a uniform normalizer. In our approach, however, $\gamma_{i,t}$ is computed at the token level to quantify contribution, thereby scaling the encouragement (or discouragement) accordingly. Specifically, we identify a set of high-flow tokens, $\mathcal{T}_{\text{high_flow}}$, using the flow computation method described earlier. We then assign higher credit to tokens within this set to emphasize the reward or penalty they receive:

$$\gamma_t = \begin{cases} \gamma_{\text{flow}} & \text{if } t \in \mathcal{T}_{\text{high_flow}} \\ 1 & \text{otherwise} \end{cases} \quad (6)$$

where $\gamma_{\text{flow}} = 1.5$ denotes the emphasis factor. This coefficient ensures that policy updates are more aggressive for tokens that genuinely contribute to the answer, thereby enabling more efficient and interpretable RL training.

4 Experiments

4.1 Experiment Settings

Backbone Models and Baselines. We employ Qwen3-4B and Qwen3-8B (Yang et al., 2025a) as our primary backbone models, with Llama families including Llama-3.1-8B and Llama-3.2-3B (Grattafiori et al., 2024) for supplementary results. We compare our method against the standard GRPO baseline and five alternative credit prioritization strategies. In these experiments, we vary only the credit assignment criteria (i.e., which tokens receive higher credits) while keeping all other settings fixed. The baselines include: 1) *Random*, serving as a neutral lower bound; 2) *Entropy* (Wang et al., 2025b), which selects tokens with high entropy; 3) *Gradient* (Green et al., 2025), which prioritizes tokens based on first-order gradient magnitude; 4) *Correlation* (Nie et al., 2025), selecting tokens with strong mutual dependencies; and 5) *Attention* (Li et al., 2025d), using maximum attention scores as a proxy for importance.

Table 2: Results of math reasoning on Qwen3-Base models. We compare performance between 1K and 8K context lengths across various methods. **Bold** denotes the best results.

Method	AIME24		AIME25		AMC23		MATH500		Olympiad		Avg.	
	1K	8K	1K	8K	1K	8K	1K	8K	1K	8K	1K	8K
<i>Qwen3-4B-Base</i>												
GRPO	8.4	19.5	5.2	16.1	55.1	57.6	74.2	81.0	42.8	49.9	37.1	44.8
Random	8.7	18.0	5.5	16.6	55.2	57.1	74.4	82.0	42.0	50.0	37.2	44.7
High-entropy	8.3	19.3	4.9	15.4	55.8	57.8	74.8	81.2	42.8	48.6	37.3	44.5
Gradient	8.6	20.3	4.2	19.6	53.2	57.8	74.1	82.3	43.3	51.3	36.7	46.3
Correlation	8.7	19.3	5.5	15.4	55.2	57.8	74.4	81.2	42.0	48.6	37.2	44.5
Attention	10.5	22.4	5.9	20.4	58.4	59.3	74.9	82.3	43.1	51.5	38.6	47.2
FlowTracer	10.9 +2.5	22.7 +3.2	6.9 +1.7	21.9 +5.8	59.0 +3.9	62.4 +4.8	75.9 +1.7	83.1 +2.1	44.2 +1.4	53.0 +3.1	39.4 +2.2	48.6 +3.8
<i>Qwen3-8B-Base</i>												
GRPO	9.3	24.9	7.3	20.8	59.1	66.3	77.1	85.1	44.2	54.4	39.4	50.3
Random	8.9	25.1	8.1	21.3	60.1	67.2	77.4	85.5	43.3	55.3	39.6	50.9
High-entropy	8.7	24.0	8.1	20.9	61.5	63.7	78.1	84.2	45.9	53.1	40.5	49.2
Gradient	9.5	23.7	8.0	20.8	60.0	65.7	77.3	84.2	45.0	53.4	40.0	49.5
Correlation	8.2	24.1	7.9	20.7	58.8	64.4	77.9	84.2	44.8	53.2	39.5	49.3
Attention	10.1	25.6	9.3	21.6	62.9	66.1	78.4	85.9	45.9	55.5	41.3	50.9
FlowTracer	13.0 +3.7	26.1 +1.2	11.8 +4.5	22.4 +1.6	65.6 +6.5	70.4 +4.1	79.7 +2.6	86.7 +1.6	46.7 +2.5	56.7 +2.3	43.4 +4.0	52.5 +2.1

Evaluation Benchmarks. We conduct experiments on three distinct task categories: (1) *Mathematical reasoning*, using five standard benchmarks: AIME24, AIME25, AMC23, MATH500 (Hendrycks et al., 2021), and OlympiadBench (He et al., 2024); (2) *Multi-domain question answering*, using *CrossThinkQA* (Aker et al., 2025), which comprises multiple-choice questions spanning various disciplines; and (3) *Domain-specific puzzle solving*, specifically the *Countdown* (Pan et al., 2025) task, where the goal is to combine four numbers with arithmetic operations to reach a target value.

Training Protocols. During training, we use a global batch size of 512 and a micro-batch size of 32, with 16 gradient accumulation steps. The learning rate is set to 1×10^{-6} , and we exclude both KL divergence and entropy regularization terms from the loss function. For trajectory sampling, we set the temperature $T = 0.99$, top- $p = 1$, and top- $k = 100$. The 3B and 4B models are trained on 8 GPUs for 500 steps, while the 8B models are trained on 16 GPUs for 600 steps. Further experimental settings are provided in Appendix C.3.

4.2 Main Results

FlowTracer consistently enhances reasoning performance across standard mathematical benchmarks.

We first evaluate the effectiveness of our method on the 1K-length setting, which represents standard chain-of-thought reasoning scenarios. As shown in Table 2 and Fig. 4, FlowTracer consistently outperforms the GRPO baseline and other token-level credit assignment heuristics across both Qwen3-4B and Qwen3-8B. Specifically, for Qwen3-8B, our method achieves an average accuracy of 43.4%, surpassing the GRPO baseline (39.4%) by a substantial margin of 4.0%. On the smaller Qwen3-4B model, our method maintains a solid lead, particularly on challenging competition-level datasets like AMC23 (+3.9%) and AIME25 (+1.7%). These results indicate that by modeling the global information flow rather than relying on point-wise signals, FlowTracer can more accurately identify and reward the pivotal reasoning steps that lead to correct solutions.

The advantage of FlowTracer becomes more pronounced in longer-context (1K→8K) reasoning scenarios. As shown in Table 2 and Fig. 4, we further investigate the method’s capability in the 8K long-context scenario, a more challenging setting where reasoning signals are significantly sparser and precise credit assignment becomes increasingly critical. As the reasoning chain lengthens, standard RL methods typically suffer from credit dilution and increased noise. However, FlowTracer demonstrates superior scalability. Notably, on Qwen3-4B, the performance gap between our method and the GRPO baseline widens from +2.2% in the 1K setting to +3.8% in the 8K setting, with a remarkable +5.8% gain on AIME25. This trend suggests that as the solution space grows complex, FlowTracer effectively locates key tokens while filtering fluent fillers, preserving the flow of credit to decisive logic steps.

Table 3: Results of the logical puzzle and question answering tasks.

Method	Countdown	CrossThinkQA
GRPO	52.6	48.0
Random	55.0	47.6
High-entropy	57.7	47.6
Attention	60.4	49.6
FlowTracer	63.2 +10.6	50.2 +2.2

Beyond standard mathematics, FlowTracer exhibits broad applicability across diverse reasoning paradigms. To verify that FlowTracer is not limited to mathematics-style reasoning, we further evaluate it on two distinct paradigms: *Countdown* (constraint-satisfying symbolic planning) and *CrossThinkQA* (multi-step logical question answering). All experiments use the same backbone Qwen3-4B-Base with 1K context window and the same RL recipe as in Table 2. As shown in Table 3, FlowTracer consistently

Table 4: Math reasoning performance on Llama families.

Method	AMC23	MATH500	Olympiad	Minerva	GSM8K	Avg
<i>Llama-3.1-8B</i>						
GRPO	3.2	8.1	3.2	5.3	18.7	7.7
Random	4.0	7.8	3.1	5.2	17.6	7.5
High-entropy	4.0	7.8	3.1	5.2	17.6	7.5
Attention	4.9	8.2	3.4	5.9	19.4	8.4
FlowTracer	5.9 +2.7	9.0 +0.9	3.7 +0.5	6.0 +0.7	21.1 +2.4	9.1 +1.4
<i>Llama-3.2-3B</i>						
GRPO	3.8	5.4	2.2	3.2	9.5	4.8
Random	3.5	5.8	2.1	3.2	9.1	4.7
High-entropy	3.8	5.2	2.3	3.1	10.0	4.9
Attention	4.0	5.9	2.4	2.9	10.4	5.1
FlowTracer	5.1 +1.3	6.7 +1.3	2.8 +0.6	3.4 +0.2	11.4 +1.9	5.9 +1.1

outperforms GRPO and point-wise heuristics, with a particularly large gain on Countdown (+10.6 absolute over GRPO), indicating that structured exploration is crucial for combinatorial planning. Meanwhile, the improvement on CrossThinkQA (+2.2) demonstrates that the same mechanism also benefits natural-language logical reasoning, supporting the generality of our approach beyond arithmetic domains.

Architecture generalization: FlowTracer transfers beyond Qwen-style backbones to the Llama family.

To examine whether our gains depend on a particular model architecture or tokenizer design, we further apply the same RL recipe to Llama-3.1-8B and Llama-3.2-3B. Since these models yield very low absolute scores on the hardest competition-level math benchmarks, we follow common practice and evaluate on a more suitable suite (AMC23, MATH500, Olympiad, MinervaMath, and GSM8K), while keeping the training protocol and compute budget unchanged. As shown in Table 4, FlowTracer consistently improves over the GRPO baseline and heuristic variants on both backbones: for Llama-3.1-8B, the average accuracy increases from 7.7% to 9.1% (+1.4), with notable gains on AMC23 (+2.7) and GSM8K (+2.4); for Llama-3.2-3B, the average rises from 4.8% to 5.9% (+1.1). These results demonstrate that our method is not tied to a specific architecture or model family, supporting its robustness as a general plug-in for reasoning-oriented RL training.

4.3 Ablation Study

Ablating token selection validates the flow score and reveals an optimal signal density. The core design choice in FlowTracer is to assign extra credit only to a subset of tokens deemed most responsible for propagating reasoning-relevant information. Table 5 thus ablates (i) *which* tokens are selected (Top- k vs. Bottom- k by flow score) and (ii) *how many* tokens receive additional credit (selection ratio). The results show a clear separation: Top- k selection consistently improves over GRPO, while prioritizing Bottom- k tokens causes substantial degradation, confirming that the flow score effectively identifies decisive reasoning tokens rather than generic filler. We further observe a density trade-off: Top-20% can under-cover the backbone and yields smaller gains, whereas Top-60% introduces noisy or redundant tokens that dilute the signal. Across all benchmarks, Top-40% provides the best overall performance, suggesting the most favorable signal-to-noise balance for credit assignment.

Reasoning flow concentrates in middle-layer attention. To locate the most informative source for flow-based credit, we exploit the hierarchical organization of transformers and ablate which layers contribute attention maps. Following Meng et al. (2022), we partition Qwen3-4B into early (0–15), middle (15–25), and late (25–35) stages, plus an all-layer baseline, and compute credit using the attention maps averaged within each subset. As shown in Fig. 6, using middle-layer attention consistently yields the best performance, suggesting that the reasoning backbone is most salient in this intermediate regime. Importantly, the all-layer average underperforms the middle-layer setting, indicating that aggregating early/late layers can dilute the critical flow signal with less task-relevant interactions. We therefore adopt middle-layer attention by default, and leave finer-grained per-layer selection and mechanistic interpretation to future work.

FlowTracer introduces only a marginal time overhead of 2.2%–4.5%. Our credit assignment method is applied between rollout and policy update: after generating a response, we run *one additional batched forward pass* to extract attention maps from mid transformer layers, compute the answer-targeted flow scores (Sec. 3.1), and select the Top-40% tokens to reweight the policy gradient. To quantify the computational overhead, we evaluate the computational cost of our method across different model sizes and context lengths in Table 6. The results show a relative overhead of 2.1%–2.2% for 1K contexts and 4.0%–4.5% for

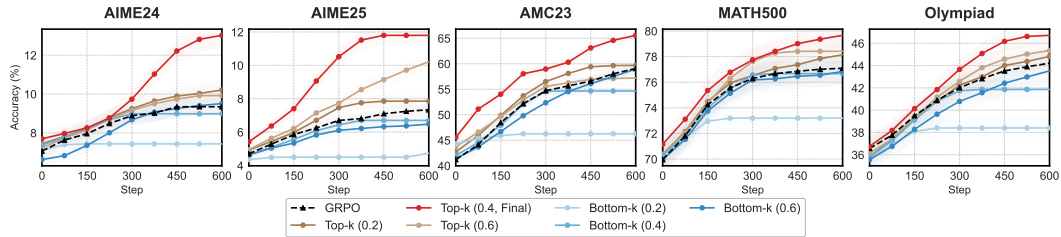


Figure 5: RL training curves of FlowTracer under different token-selection ratios, comparing Top-k vs. Bottom-k (by flow score).

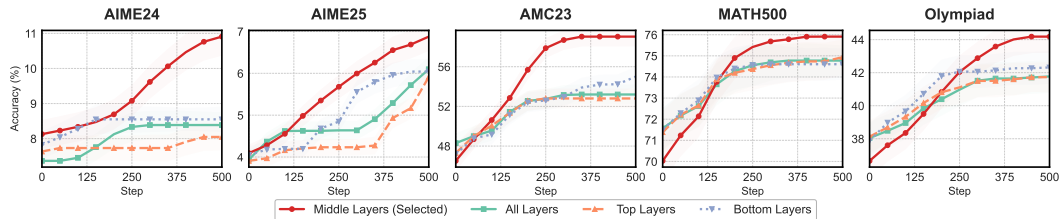


Figure 6: FlowTracer using attention signals from different layer ranges on Qwen3-4B with 1024 context length on math reasoning.

Table 5: Performance comparison for different variants of FlowTracer. The final chosen setting (Top-k with $k = 0.4$) is highlighted in blue. Best performance in each column is in bold.

Method	AIME24	AIME25	AMC23	MATH500	Olympiad	Avg
GRPO	9.3	7.3	59.1	77.1	44.2	39.4
Top-20%	10.2	7.9	59.7	78.1	44.8	40.1
Top-40%	13.0	11.8	65.6	79.7	46.7	43.4
Top-60%	9.9	10.2	57.2	78.4	45.3	40.2
Bottom-20%	7.4	4.7	46.2	73.2	38.4	34.0
Bottom-40%	9.0	6.7	54.7	76.7	41.9	37.8
Bottom-60%	9.5	6.5	58.9	76.8	43.5	39.1

Table 6: Computational Overhead Analysis. Average training step time and FlowTracer’s credit assignment time across different model sizes and context lengths.

Model	Context	Step Time	Flow Credit	Overhead
Qwen3-4B	1K	71.0 s	1.57 s	2.2%
	8K	189.7 s	8.55 s	4.5%
Qwen3-8B	1K	79.0 s	1.66 s	2.1%
	8K	275.3 s	11.04 s	4.0%

8K contexts. Since FlowTracer requires only a single additional batched forward pass over the generated sequence, its computational cost is overshadowed by the much larger expense of autoregressive token-by-token sampling.

5 Additional Analysis and Limitations

5.1 Why Not Continuous Credit Assignment?

FlowTracer converts token flow throughput into a **hard credit mask**: after computing token-level flow, it selects the Top-40% tokens and multiplies their GRPO surrogate terms by γ_{flow} . An alternative is to use flow continuously, either by (i) scaling each token directly with its raw or transformed flow value, or by (ii) selecting tokens until their cumulative flow mass reaches a prescribed threshold. However, we found these alternatives consistently less stable. The key empirical reason is that **flow throughput is highly skewed**: a small number of tokens carry a large fraction of total flow, while most tokens have very small values.

Table 7 provides three insights: (1) **Flow is more reliable as a ranking signal than as a calibrated continuous weight**. Raw-flow reweighting severely amplifies outliers, and transformations such as Sigmoid and Log1p improve stability but still underperform hard Top-40% reweighting. (2) **High-**

Table 7: Ablations on continuous credit assignment using Qwen3-4B with 1K context length. Bold denotes the best performance.

Method	AIME24	AIME25	AMC23	MATH500	Olympiad	Avg.
GRPO	8.4	5.2	55.1	74.2	42.8	37.1
<i>Hard Top-40% reweighting with different scaling factors ($\gamma_{\text{flow}} = 1.5$ chosen)</i>						
$\gamma_{\text{flow}} = 0.5$	7.8	3.3	53.3	75.3	40.8	36.1
$\gamma_{\text{flow}} = 1.2$	8.9	5.5	58.0	76.0	42.6	38.2
$\gamma_{\text{flow}} = 1.5$	10.9	6.9	59.0	75.9	44.2	39.4
$\gamma_{\text{flow}} = 1.8$	8.7	4.3	57.9	74.9	43.3	37.8
$\gamma_{\text{flow}} = 2.0$	5.9	4.4	49.5	69.9	36.9	33.3
$\gamma_{\text{flow}} = 3.0$	6.0	3.9	41.0	64.1	33.5	29.7
<i>vs. continuous reweighting</i>						
Raw Flow	6.8	3.1	37.9	63.0	32.7	28.7
Tanh+Z-score	6.6	3.8	42.7	74.0	42.2	33.9
Sigmoid	9.0	5.1	56.5	74.5	40.3	37.1
MAD	7.4	6.2	54.8	63.8	35.1	33.5
Log1p	9.4	5.3	57.0	75.4	40.1	37.4
<i>vs. soft dynamic thresholding</i>						
Soft 20% flow	7.4	3.5	46.0	71.5	36.8	33.0
Soft 40% flow	9.1	4.8	51.8	73.6	41.4	36.1
Soft 60% flow	8.5	4.3	53.0	73.8	42.2	36.4
Soft 80% flow	8.3	4.2	55.0	72.5	40.8	36.2

flow tokens should be emphasized moderately rather than exclusively. The best result is obtained around $\gamma_{\text{flow}} = 1.5$; smaller values do not sufficiently distinguish the reasoning backbone, while larger values also degrade performance. (3) **Selecting by a fixed token ratio is more robust than selecting by cumulative flow mass.** Since flow mass is highly concentrated, cumulative thresholds either under-cover the backbone or dilute it with low-flow tokens. **Overall, the hard Top-40% rule acts as a simple denoising step:** it preserves the ordinal information in flow throughput while avoiding the instability of using its heavy-tailed magnitude directly.

5.2 Answer-Format Robustness and Structural-vs-Semantic Contributions

We further check whether the flow signal is sensitive to answer formatting or driven by specific token types. For answer formatting, although all main experiments define the answer region with `\boxed{\}`, we vary the *answer form inside this region*. The Top-40% high-flow set remains almost unchanged: its overlap with the answer-only format is 1.00 for full-line and explanation-augmented answers, and 0.93 for multiple-choice outputs. Thus, **the flow signal is robust to answer-format variations rather than tied to a brittle answer string.**

For token types, we split tokens into structural delimiters and semantic-content tokens, select the Top-40% high-flow tokens within each subset, and apply the same credit rule. Structural delimiters recover most of the full gain (38.8% vs. 39.4%), whereas semantic-content tokens provide a smaller improvement (37.6%). Thus, **structural delimiters dominate the improvement, with semantic-content tokens adding a smaller complementary gain.** Full results are in Appendix D.2.

5.3 Scope of Attention-Based Flow and Limitations

FlowTracer does not claim that attention fully explains LLM reasoning. Our use of attention is narrower: it provides an explicit token-to-token interaction graph from which answer-directed routing signals can be extracted. Raw attention contains both useful structure and noise, and FlowTracer filters it into an answer--targeted, flow--conserving multi-hop backbone more useful for analysis and RL credit assignment than raw weights alone.

Several limitations suggest future directions. First, FlowTracer currently assumes a localized answer region; extending it to open-ended generation or tool-call trajectories requires more flexible target definitions. Second, outcome-only rewards cannot always separate locally useful intermediate reasoning from reasoning that supports a wrong final answer, making FlowTracer complementary to PRM-style process supervision. Third, very long contexts may introduce noisier attention graphs, motivating adaptive flow extraction for 16K/24K or longer contexts.

6 Conclusion

This work tries to address the critical challenge of credit assignment in RL4LLM by moving beyond uniform rewards and point-wise heuristics that treat tokens in isolation. We propose **FlowTracer**, a framework that leverages the model’s internal attention signals to reconstruct the global structure of information propagation. By modeling the reasoning process as a directed flow network, we effectively identify the “reasoning backbone”, distinguishing decisive steps from routine filler based on their actual contribution to the answer. Our results demonstrate that shaping rewards with these flow-based importances enables the learning signal to focus precisely on high-impact tokens, delivering consistent performance gains across complex reasoning tasks. Finally, this work suggests that the internal geometry of attention within LLMs offers a powerful, structural signal for more efficient and interpretable model alignment.

Acknowledgments

This work was in part supported by Scientific Research Innovation Capability Support Project for Young Faculty (U40) of the Ministry of Education of China (SRICSPYF-ZY2025019), NSFC 625B2119 and Alibaba Group.

References

- Josh Achiam, Steven Adler, Sandhini Agarwal, Lama Ahmad, Ilge Akkaya, Florencia Leoni Aleman, Diogo Almeida, Janko Altenschmidt, Sam Altman, Shyamal Anadkat, et al. Gpt-4 technical report. *arXiv preprint arXiv:2303.08774*, 2023.
- Syeda Nahida Akter, Shrimai Prabhunoye, Matvei Novikov, Seungju Han, Ying Lin, Evelina Bakhturina, Eric Nyberg, Yejin Choi, Mostofa Patwary, Mohammad Shoeybi, et al. Nemotron-crossthink: Scaling self-learning beyond math reasoning. *arXiv preprint arXiv:2504.13941*, 2025.
- Emmanuel Ameisen, Jack Lindsey, Adam Pearce, Wes Gurnee, Nicholas L Turner, Brian Chen, Craig Citro, David Abrahams, Shan Carter, Basil Hosmer, et al. Circuit tracing: Revealing computational graphs in language models. *Transformer Circuits Thread*, 6:16318–16352, 2025.
- Yuntao Bai, Andy Jones, Kamal Ndousse, Amanda Askell, Anna Chen, Nova DasSarma, Dawn Drain, Stanislav Fort, Deep Ganguli, Tom Henighan, et al. Training a helpful and harmless assistant with reinforcement learning from human feedback. *arXiv preprint arXiv:2204.05862*, 2022.
- Nora Belrose, Zach Furman, Logan Smith, Danny Halawi, Igor Ostrovsky, Lev McKinney, Stella Biderman, and Jacob Steinhardt. Eliciting latent predictions from transformers with the tuned lens. *arXiv preprint arXiv:2303.08112*, 2023.
- Leonardo Bertolazzi, Philipp Mondorf, Barbara Plank, and Raffaella Bernardi. The validation gap: A mechanistic analysis of how language models compute arithmetic but fail to validate it. In *Proceedings of the 2025 Conference on Empirical Methods in Natural Language Processing*, pp. 29375–29412, 2025.
- Paul C Bogdan, Uzay Macar, Neel Nanda, and Arthur Conmy. Thought anchors: Which llm reasoning steps matter? *arXiv preprint arXiv:2506.19143*, 2025.
- Collin Burns, Haotian Ye, Dan Klein, and Jacob Steinhardt. Discovering latent knowledge in language models without supervision. *arXiv preprint arXiv:2212.03827*, 2022.
- Vivien Cabannes, Charles Arnal, Wassim Bouaziz, Xingyu Yang, Francois Charton, and Julia Kempe. Iteration head: A mechanistic study of chain-of-thought. *Advances in Neural Information Processing Systems*, 37:109101–109122, 2024.
- Lvda Chen, Yang Li, and Junchi Yan. Maskco: Masked generation drives effective representation learning and exploiting for combinatorial optimization. In *The Fourteenth International Conference on Learning Representations*, 2026.
- Qiguang Chen, Libo Qin, Jiaqi Wang, Jinxuan Zhou, and Wanxiang Che. Unlocking the capabilities of thought: A reasoning boundary framework to quantify and optimize chain-of-thought. *Advances in Neural Information Processing Systems*, 37:54872–54904, 2024.
- Daixuan Cheng, Shaohan Huang, Xuekai Zhu, Bo Dai, Wayne Xin Zhao, Zhenliang Zhang, and Furu Wei. Reasoning with exploration: An entropy perspective. *arXiv preprint arXiv:2506.14758*, 2025a.
- Jie Cheng, Gang Xiong, Ruixi Qiao, Lijun Li, Chao Guo, Junle Wang, Yisheng Lv, and Fei-Yue Wang. Stop summation: Min-form credit assignment is all process reward model needs for reasoning. *arXiv preprint arXiv:2504.15275*, 2025b.
- Paul F Christiano, Jan Leike, Tom Brown, Miljan Martic, Shane Legg, and Dario Amodei. Deep reinforcement learning from human preferences. *Advances in neural information processing systems*, 30, 2017.
- Karl Cobbe, Vineet Kosaraju, Mohammad Bavarian, Mark Chen, Heewoo Jun, Lukasz Kaiser, Matthias Plappert, Jerry Tworek, Jacob Hilton, Reiichiro Nakano, Christopher Hesse, and John Schulman. Training verifiers to solve math word problems. *arXiv preprint arXiv:2110.14168*, 2021.
- Ganqu Cui, Yuchen Zhang, Jiacheng Chen, Lifan Yuan, Zhi Wang, Yuxin Zuo, Haozhan Li, Yuchen Fan, Huayu Chen, Weize Chen, et al. The entropy mechanism of reinforcement learning for reasoning language models. *arXiv preprint arXiv:2505.22617*, 2025.
- Zhichen Dong, Zhanhui Zhou, Chao Yang, Jing Shao, and Yu Qiao. Attacks, defenses and evaluations for llm conversation safety: A survey. In *Proceedings of the 2024 Conference of the North American Chapter of the Association for Computational Linguistics: Human Language Technologies (Volume 1: Long Papers)*, pp. 6734–6747, 2024.

-
- Zhichen Dong, Zhanhui Zhou, Zhixuan Liu, Chao Yang, and Chaochao Lu. Emergent response planning in llms. *arXiv preprint arXiv:2502.06258*, 2025.
- Razvan-Gabriel Dumitru, Paul Ioan Clotan, Vikas Yadav, Darius Peteleaza, and Mihai Surdeanu. Change is the only constant: Dynamic llm slicing based on layer redundancy. In *Findings of the Association for Computational Linguistics: EMNLP 2024*, pp. 9912–9920, 2024.
- Subhabrata Dutta, Joykirat Singh, Soumen Chakrabarti, and Tanmoy Chakraborty. How to think step-by-step: A mechanistic understanding of chain-of-thought reasoning. *arXiv preprint arXiv:2402.18312*, 2024.
- Kanishk Gandhi, Ayush Chakravarthy, Anikait Singh, Nathan Lile, and Noah D Goodman. Cognitive behaviors that enable self-improving reasoners, or, four habits of highly effective stars. *arXiv preprint arXiv:2503.01307*, 2025.
- Mor Geva, Jasmijn Bastings, Katja Filippova, and Amir Globerson. Dissecting recall of factual associations in auto-regressive language models. In *Proceedings of the 2023 Conference on Empirical Methods in Natural Language Processing*, pp. 12216–12235, 2023.
- Aaron Grattafiori, Abhimanyu Dubey, Abhinav Jauhri, Abhinav Pandey, Abhishek Kadian, Ahmad Al-Dahle, Aiesha Letman, Akhil Mathur, Alan Schelten, Alex Vaughan, et al. The llama 3 herd of models. *arXiv preprint arXiv:2407.21783*, 2024.
- Annabel Green, Andrew Delta, Carter Wilson, Eleanor Wragge, Andrew Scolto, and Benedict Wickersham. Contextual gradient recomposition for sequential coherence preservation in large language model token generation. ResearchGate preprint, August 2025. Preprint.
- Xinyu Guan, Li Lyna Zhang, Yifei Liu, Ning Shang, Youran Sun, Yi Zhu, Fan Yang, and Mao Yang. rstar-math: Small llms can master math reasoning with self-evolved deep thinking. *arXiv preprint arXiv:2501.04519*, 2025.
- Daya Guo, Dejian Yang, Haowei Zhang, Junxiao Song, Ruoyu Zhang, Runxin Xu, Qihao Zhu, Shirong Ma, Peiyi Wang, Xiao Bi, et al. Deepseek-r1: Incentivizing reasoning capability in llms via reinforcement learning. *arXiv preprint arXiv:2501.12948*, 2025.
- Chaoqun He, Renjie Luo, Yuzhuo Bai, Shengding Hu, Zhen Leng Thai, Junhao Shen, Jinyi Hu, Xu Han, Yujie Huang, Yuxiang Zhang, et al. Olympiadbench: A challenging benchmark for promoting agi with olympiad-level bilingual multimodal scientific problems. *arXiv preprint arXiv:2402.14008*, 2024.
- Dan Hendrycks, Collin Burns, Saurav Kadavath, Akul Arora, Steven Basart, Eric Tang, Dawn Song, and Jacob Steinhardt. Measuring mathematical problem solving with the math dataset. *arXiv preprint arXiv:2103.03874*, 2021.
- Evan Hernandez, Belinda Z Li, and Jacob Andreas. Inspecting and editing knowledge representations in language models. *arXiv preprint arXiv:2304.00740*, 2023.
- Binyuan Hui, Jian Yang, Zeyu Cui, Jiayi Yang, Dayiheng Liu, Lei Zhang, Tianyu Liu, Jiajun Zhang, Bowen Yu, Kai Dang, et al. Qwen2. 5-coder technical report. *arXiv preprint arXiv:2409.12186*, 2024.
- Aaron Jaech, Adam Kalai, Adam Lerer, Adam Richardson, Ahmed El-Kishky, Aiden Low, Alec Hel-yar, Aleksander Madry, Alex Beutel, Alex Carney, et al. Openai o1 system card. *arXiv preprint arXiv:2412.16720*, 2024.
- Ziwei Ji, Delong Chen, Etsuko Ishii, Samuel Cahyawijaya, Yejin Bang, Bryan Wilie, and Pascale Fung. Llm internal states reveal hallucination risk faced with a query. *arXiv preprint arXiv:2407.03282*, 2024.
- Muhammad Khalifa, Rishabh Agarwal, Lajanugen Logeswaran, Jaekyeom Kim, Hao Peng, Moontae Lee, Honglak Lee, and Lu Wang. Process reward models that think. *arXiv preprint arXiv:2504.16828*, 2025.
- Nathan Lambert, Jacob Morrison, Valentina Pyatkin, Shengyi Huang, Hamish Ivison, Faeze Brahman, Lester James V Miranda, Alisa Liu, Nouha Dziri, Shane Lyu, et al. Tulu 3: Pushing frontiers in open language model post-training. *arXiv preprint arXiv:2411.15124*, 2024.
- Dacheng Li, Shiyi Cao, Tyler Griggs, Shu Liu, Xiangxi Mo, Eric Tang, Sumanth Hegde, Kourosh Hakhmaneshi, Shishir G Patil, Matei Zaharia, et al. Llms can easily learn to reason from demonstrations structure, not content, is what matters! *arXiv preprint arXiv:2502.07374*, 2025a.
- Hengli Li, Chenxi Li, Tong Wu, Xuekai Zhu, Yuxuan Wang, Zhaoxin Yu, Eric Hanchen Jiang, Song-Chun Zhu, Zixia Jia, Ying Nian Wu, et al. Seek in the dark: Reasoning via test-time instance-level policy gradient in latent space. *arXiv preprint arXiv:2505.13308*, 2025b.

-
- Kenneth Li, Aspen K Hopkins, David Bau, Fernanda Viégas, Hanspeter Pfister, and Martin Wattenberg. Emergent world representations: Exploring a sequence model trained on a synthetic task. *arXiv preprint arXiv:2210.13382*, 2022.
- Pengyi Li, Matvey Skripkin, Alexander Zubrey, Andrey Kuznetsov, and Ivan Oseledets. Confidence is all you need: Few-shot rl fine-tuning of language models. *arXiv preprint arXiv:2506.06395*, 2025c.
- Yang Li, Zhichen Dong, Yuhan Sun, Weixun Wang, Shaopan Xiong, Yijia Luo, Jiashun Liu, Han Lu, Jiamang Wang, Wenbo Su, et al. Attention illuminates llm reasoning: The preplan-and-anchor rhythm enables fine-grained policy optimization. *arXiv preprint arXiv:2510.13554*, 2025d.
- Yang Li, Jiale Ma, Wenzheng Pan, Runzhong Wang, Haoyu Geng, Nianzu Yang, and Junchi Yan. Unify ml4tsp: Drawing methodological principles for tsp and beyond from streamlined design space of learning and search. In *The Thirteenth International Conference on Learning Representations*, 2025e.
- Yang Li, Jiale Ma, Yebin Yang, Qitian Wu, Hongyuan Zha, and Junchi Yan. Generative modeling reinvents supervised learning: Label repurposing with predictive consistency learning. In *Forty-second International Conference on Machine Learning*, 2025f.
- Yang Li, Lvda Chen, Haonan Wang, Runzhong Wang, and Junchi Yan. Generation as search operator for test-time scaling of diffusion-based combinatorial optimization. *Advances in Neural Information Processing Systems*, 38:127168–127196, 2026.
- Hunter Lightman, Vineet Kosaraju, Yuri Burda, Harrison Edwards, Bowen Baker, Teddy Lee, Jan Leike, John Schulman, Ilya Sutskever, and Karl Cobbe. Let’s verify step by step. In *The Twelfth International Conference on Learning Representations*, 2023.
- Zicheng Lin, Tian Liang, Jiahao Xu, Qiuzhi Lin, Xing Wang, Ruilin Luo, Chufan Shi, Siheng Li, Yujia Yang, and Zhaopeng Tu. Critical tokens matter: Token-level contrastive estimation enhances llm’s reasoning capability. *arXiv preprint arXiv:2411.19943*, 2024.
- Jiashun Liu, Johan Obando-Ceron, Han Lu, Yancheng He, Weixun Wang, Wenbo Su, Bo Zheng, Pablo Samuel Castro, Aaron Courville, and Ling Pan. Asymmetric proximal policy optimization: mini-critics boost llm reasoning. *arXiv preprint arXiv:2510.01656*, 2025.
- Yuze Liu, Chaochao Lu, and Chao Yang. Shadow: Dynamic-aware credit assignment against long-horizon tasks. In *Proceedings of the AAAI Conference on Artificial Intelligence*, volume 40, pp. 23935–23944, 2026.
- Rujiao Long, Yang Li, Xingyao Zhang, Weixun Wang, Tianqianjin Lin, Xi Zhao, Yuchi Xu, Wenbo Su, Junchi Yan, and Bo Zheng. Reasoning palette: Modulating reasoning via latent contextualization for controllable exploration for (v) lms. *arXiv preprint arXiv:2512.17206*, 2025.
- Han Lu, Zichen Liu, Shaopan Xiong, Yancheng He, Wei Gao, Yanan Wu, Weixun Wang, Jiashun Liu, Yang Li, Haizhou Zhao, et al. Part ii: Roll flash—accelerating rlvr and agentic training with asynchrony. *arXiv preprint arXiv:2510.11345*, 2025.
- Kevin Meng, David Bau, Alex Andonian, and Yonatan Belinkov. Locating and editing factual associations in gpt. *Advances in neural information processing systems*, 35:17359–17372, 2022.
- Yu Meng, Mengzhou Xia, and Danqi Chen. Simpo: Simple preference optimization with a reference-free reward. *Advances in Neural Information Processing Systems*, 37:124198–124235, 2024.
- Gouki Minegishi, Hiroki Furuta, Takeshi Kojima, Yusuke Iwasawa, and Yutaka Matsuo. Topology of reasoning: Understanding large reasoning models through reasoning graph properties. *arXiv preprint arXiv:2506.05744*, 2025.
- Hosein Mohebbi, Willem Zuidema, Grzegorz Chrupala, and Afra Alishahi. Quantifying context mixing in transformers. In *Proceedings of the 17th Conference of the European Chapter of the Association for Computational Linguistics*, pp. 3378–3400, 2023.
- Zhijie Nie, Richong Zhang, and Zhanyu Wu. A text is worth several tokens: Text embedding from llms secretly aligns well with the key tokens. In *Proceedings of the 63rd Annual Meeting of the Association for Computational Linguistics (Volume 1: Long Papers)*, pp. 7683–7694, 2025.
- Long Ouyang, Jeffrey Wu, Xu Jiang, Diogo Almeida, Carroll Wainwright, Pamela Mishkin, Chong Zhang, Sandhini Agarwal, Katarina Slama, Alex Ray, et al. Training language models to follow instructions with human feedback. *Advances in neural information processing systems*, 35:27730–27744, 2022.

-
- Jiayi Pan, Junjie Zhang, Xingyao Wang, Lifan Yuan, Hao Peng, and Alane Suhr. Tinyzero. <https://github.com/Jiayi-Pan/TinyZero>, 2025. Accessed: 2025-01-24.
- Chen Qian, Dongrui Liu, Haochen Wen, Zhen Bai, Yong Liu, and Jing Shao. Demystifying reasoning dynamics with mutual information: Thinking tokens are information peaks in llm reasoning. *arXiv preprint arXiv:2506.02867*, 2025.
- Rafael Rafailov, Archit Sharma, Eric Mitchell, Christopher D Manning, Stefano Ermon, and Chelsea Finn. Direct preference optimization: Your language model is secretly a reward model. *Advances in neural information processing systems*, 36:53728–53741, 2023.
- Jie Ren, Qipeng Guo, Hang Yan, Dongrui Liu, Quanshi Zhang, Xipeng Qiu, and Dahua Lin. Identifying semantic induction heads to understand in-context learning. In *Findings of the Association for Computational Linguistics: ACL 2024*, pp. 6916–6932, 2024.
- John Schulman, Philipp Moritz, Sergey Levine, Michael Jordan, and Pieter Abbeel. High-dimensional continuous control using generalized advantage estimation. *arXiv preprint arXiv:1506.02438*, 2015.
- Zhihong Shao, Peiyi Wang, Qihao Zhu, Runxin Xu, Junxiao Song, Xiao Bi, Haowei Zhang, Mingchuan Zhang, YK Li, Yang Wu, et al. Deepseekmath: Pushing the limits of mathematical reasoning in open language models. *arXiv preprint arXiv:2402.03300*, 2024.
- Kimi Team, Yifan Bai, Yiping Bao, Y Charles, Cheng Chen, Guanduo Chen, Haiting Chen, Huarong Chen, Jiahao Chen, Ningxin Chen, et al. Kimi k2: Open agentic intelligence. *arXiv preprint arXiv:2507.20534*, 2025a.
- Kimi Team, Angang Du, Bofei Gao, Bofei Xing, Changjiu Jiang, Cheng Chen, Cheng Li, Chenjun Xiao, Chenzhuang Du, Chonghua Liao, et al. Kimi k1. 5: Scaling reinforcement learning with llms. *arXiv preprint arXiv:2501.12599*, 2025b.
- Alexander Matt Turner, Lisa Thiergart, Gavin Leech, David Udell, Juan J Vazquez, Ulisse Mini, and Monte MacDiarmid. Steering language models with activation engineering. *arXiv preprint arXiv:2308.10248*, 2023.
- Jean Vassoyan, Nathanaël Beau, and Roman Plaud. Ignore the kl penalty! boosting exploration on critical tokens to enhance rl fine-tuning. *arXiv preprint arXiv:2502.06533*, 2025.
- Constantin Venhoff, Iván Arcuschin, Philip Torr, Arthur Conmy, and Neel Nanda. Understanding reasoning in thinking language models via steering vectors. *arXiv preprint arXiv:2506.18167*, 2025.
- Jiawei Wang, Jiakai Liu, Yuqian Fu, Yingru Li, Xintao Wang, Yuan Lin, Yu Yue, Lin Zhang, Yang Wang, and Ke Wang. Harnessing uncertainty: Entropy-modulated policy gradients for long-horizon llm agents. *arXiv preprint arXiv:2509.09265*, 2025a.
- Peiyi Wang, Lei Li, Zhihong Shao, Runxin Xu, Damai Dai, Yifei Li, Deli Chen, Yu Wu, and Zhifang Sui. Math-shepherd: Verify and reinforce llms step-by-step without human annotations. In *Proceedings of the 62nd Annual Meeting of the Association for Computational Linguistics (Volume 1: Long Papers)*, pp. 9426–9439, 2024.
- Shenzhi Wang, Le Yu, Chang Gao, Chujie Zheng, Shixuan Liu, Rui Lu, Kai Dang, Xionghui Chen, Jianxin Yang, Zhenru Zhang, et al. Beyond the 80/20 rule: High-entropy minority tokens drive effective reinforcement learning for llm reasoning. *arXiv preprint arXiv:2506.01939*, 2025b.
- Weixun Wang, Shaopan Xiong, Gengru Chen, Wei Gao, Sheng Guo, Yancheng He, Ju Huang, Jiaheng Liu, Zhendong Li, Xiaoyang Li, et al. Reinforcement learning optimization for large-scale learning: An efficient and user-friendly scaling library. *arXiv preprint arXiv:2506.06122*, 2025c.
- Weixun Wang, XiaoXiao Xu, Wanhe An, Fangwen Dai, Wei Gao, Yancheng He, Ju Huang, Qiang Ji, Hanqi Jin, Xiaoyang Li, et al. Let it flow: Agentic crafting on rock and roll, building the rome model within an open agentic learning ecosystem. *arXiv preprint arXiv:2512.24873*, 2025d.
- Yu Wang, Yang Li, Jiale Ma, Junchi Yan, and Yi Chang. Nexco: Native solution expansion for diffusion-based combinatorial optimization. In *The Fourteenth International Conference on Learning Representations*, 2026.
- Guofu Xie, Yunsheng Shi, Hongtao Tian, Ting Yao, and Xiao Zhang. Capo: Towards enhancing llm reasoning through verifiable generative credit assignment. *arXiv e-prints*, pp. arXiv–2508, 2025.

-
- Huajian Xin, ZZ Ren, Junxiao Song, Zhihong Shao, Wanjia Zhao, Haocheng Wang, Bo Liu, Liyue Zhang, Xuan Lu, Qiushi Du, et al. Deepseek-prover-v1. 5: Harnessing proof assistant feedback for reinforcement learning and monte-carlo tree search. In *International Conference on Learning Representations*, volume 2025, pp. 72274–72303, 2025.
- An Yang, Anfeng Li, Baosong Yang, Beichen Zhang, Binyuan Hui, Bo Zheng, Bowen Yu, Chang Gao, Chengen Huang, Chenxu Lv, et al. Qwen3 technical report. *arXiv preprint arXiv:2505.09388*, 2025a.
- John Yang, Carlos E Jimenez, Alexander Wettig, Kilian Lieret, Shunyu Yao, Karthik Narasimhan, and Ofir Press. Swe-agent: Agent-computer interfaces enable automated software engineering. *Advances in Neural Information Processing Systems*, 37:50528–50652, 2024.
- Zhihe Yang, Xufang Luo, Zilong Wang, Dongqi Han, Zhiyuan He, Dongsheng Li, and Yunjian Xu. Do not let low-probability tokens over-dominate in rl for llms. *arXiv preprint arXiv:2505.12929*, 2025b.
- Qiyang Yu, Zheng Zhang, Ruofei Zhu, Yufeng Yuan, Xiaochen Zuo, Yu Yue, Weinan Dai, Tiantian Fan, Gaohong Liu, Lingjun Liu, et al. Dapo: An open-source llm reinforcement learning system at scale. *arXiv preprint arXiv:2503.14476*, 2025.
- Yiran Zhao, Wenxuan Zhang, Yuxi Xie, Anirudh Goyal, Kenji Kawaguchi, and Michael Shieh. Identifying and tuning safety neurons in large language models. In *The Thirteenth International Conference on Learning Representations*, 2025b. URL <https://openreview.net/forum>, 2025.
- Chujie Zheng, Shixuan Liu, Mingze Li, Xiong-Hui Chen, Bowen Yu, Chang Gao, Kai Dang, Yuqiong Liu, Rui Men, An Yang, et al. Group sequence policy optimization. *arXiv preprint arXiv:2507.18071*, 2025.
- Zifan Zheng, Yezhaohui Wang, Yuxin Huang, Shichao Song, Mingchuan Yang, Bo Tang, Feiyu Xiong, and Zhiyu Li. Attention heads of large language models: A survey. *arXiv preprint arXiv:2409.03752*, 2024.
- Zhanhui Zhou, Jie Liu, Zhichen Dong, Jiaheng Liu, Chao Yang, Wanli Ouyang, and Yu Qiao. Emulated disalignment: Safety alignment for large language models may backfire! In *Proceedings of the 62nd Annual Meeting of the Association for Computational Linguistics (Volume 1: Long Papers)*, pp. 15810–15830, 2024a.
- Zhanhui Zhou, Zhixuan Liu, Jie Liu, Zhichen Dong, Chao Yang, and Yu Qiao. Weak-to-strong search: Align large language models via searching over small language models. *Advances in Neural Information Processing Systems*, 37:4819–4851, 2024b.
- Daniel M Ziegler, Nisan Stiennon, Jeffrey Wu, Tom B Brown, Alec Radford, Dario Amodei, Paul Christiano, and Geoffrey Irving. Fine-tuning language models from human preferences. *arXiv preprint arXiv:1909.08593*, 2019.
- Andy Zou, Long Phan, Sarah Chen, James Campbell, Phillip Guo, Richard Ren, Alexander Pan, Xuwang Yin, Mantas Mazeika, Ann-Kathrin Dombrowski, et al. Representation engineering: A top-down approach to ai transparency. *arXiv preprint arXiv:2310.01405*, 2023.

A Preliminaries

A.1 Information Propagation in Decoder-Only LLMs

We consider an L -layer decoder-only LLM $\pi_\theta(\mathbf{y} \mid \mathbf{x})$ that generates a response \mathbf{y} given a prompt \mathbf{x} . At any decoding step, the model processes the concatenated sequence $\mathcal{S} = (\mathbf{x}, \mathbf{y}_{<t})$ of length N . As the model processes tokens, it maintains an information stream encoded in hidden states $\mathbf{H}^{(l)} \in \mathbb{R}^{N \times d}$, where d is the model dimension.

The primary engine for routing information between tokens is the Multi-Head Self-Attention (MHSA) mechanism. Within a specific layer l and head h , the input representation $\mathbf{H}^{(l-1)}$ is first projected into queries, keys, and values using learnable weight matrices $W_Q^{(h)}, W_K^{(h)}, W_V^{(h)} \in \mathbb{R}^{d \times d_k}$:

$$Q^{(h)} = \mathbf{H}^{(l-1)}W_Q^{(h)}, K^{(h)} = \mathbf{H}^{(l-1)}W_K^{(h)}, V^{(h)} = \mathbf{H}^{(l-1)}W_V^{(h)} \quad (7)$$

The flow of information from previous tokens to the current token is determined by the attention matrix $A^{(h,l)} \in \mathbb{R}^{N \times N}$, computed as:

$$A^{(h,l)} = \text{softmax} \left(\frac{Q^{(h)}(K^{(h)})^\top}{\sqrt{d_k}} + M \right) \quad (8)$$

where M is a causal mask (setting $M_{i,j} = -\infty$ for $j > i$) ensuring that token i can only gather information from preceding tokens $j \leq i$. The output of the attention head, $O^{(h)} = A^{(h,l)}V^{(h)}$, represents a weighted aggregation of values from the context. These head outputs are aggregated and processed via a Feed-Forward Network (FFN) with residual connections to yield a refined state $\mathbf{H}^{(l)}$ enriched by global context:

$$\mathbf{H}^{(l)} = \mathbf{H}^{(l-1)} + \text{FFN}(\mathbf{H}^{(l-1)} + \text{Concat}(O^{(1)}, \dots, O^{(H)})W_O) \quad (9)$$

Among these components, the attention matrix $A^{(h,l)}$ serves as the explicit control mechanism for data routing. The scalar entry $A_{i,j}^{(h,l)}$ directly quantifies the proportion of information token i retrieves from token j , providing the most natural perspective for analyzing the topology of global information flow.

A.2 Reinforcement Learning with Verifiable Rewards

Reinforcement Learning with Verifiable Rewards (RLVR) optimizes an LLM policy π_θ to generate a solution \mathbf{y} for a prompt \mathbf{x} , guided by a sparse scalar reward $r(\mathbf{x}, \mathbf{y})$ (e.g., correctness in math or coding). Standard approaches, such as Proximal Policy Optimization (PPO), rely on a value function critic to estimate the expected return, which incurs significant computational and memory overheads.

Group Relative Policy Optimization (GRPO) eliminates the need for a critic by using group statistics as the baseline. For each query, GRPO samples a group of G outputs $\{\mathbf{y}_1, \dots, \mathbf{y}_G\}$ from the old policy $\pi_{\theta_{\text{old}}}$. The advantage for the i -th output is estimated as:

$$\hat{A}_i = \frac{r_i - \text{mean}(\{r_j\})}{\text{std}(\{r_j\})} \quad (10)$$

The policy is updated by maximizing a generalized surrogate objective that aggregates gradients over all tokens, incorporating a token-wise importance coefficient $\gamma_{i,t}$:

$$\mathcal{J}(\theta) = \mathbb{E}_{\mathbf{x} \sim \mathcal{D}} \left[\frac{1}{G} \sum_{i=1}^G \frac{1}{N_i} \sum_{t=1}^{N_i} \gamma_{i,t} \cdot \min \left(\frac{\pi_\theta(y_{i,t} \mid \mathbf{x}, \mathbf{y}_{i,<t})}{\pi_{\theta_{\text{old}}}(y_{i,t} \mid \mathbf{x}, \mathbf{y}_{i,<t})} \hat{A}_i, \right. \right. \\ \left. \left. \text{clip} \left(\frac{\pi_\theta(y_{i,t} \mid \mathbf{x}, \mathbf{y}_{i,<t})}{\pi_{\theta_{\text{old}}}(y_{i,t} \mid \mathbf{x}, \mathbf{y}_{i,<t})}, 1 - \epsilon, 1 + \epsilon \right) \hat{A}_i \right) \right] \quad (11)$$

In standard GRPO, the importance coefficient is set uniformly as $\gamma_{i,t} = 1$, assigning uniform credit to every token regardless of its semantic role. Recent studies suggest that RLVR performance can be significantly improved by leveraging fine-grained, token-wise signals that distinguish critical reasoning steps from trivial tokens, a capability we explore in subsequent sections.

B Model and Dataset Specification

Model Specification. In this work, we take Qwen3-4B and Qwen3-8B (Yang et al., 2025a) as the main backbones for our primary experiments. To further validate the generalization of our method, we also

provide supplementary experimental results using Llama-3.1-8B and Llama-3.2-3B (Grattafiori et al., 2024). The detailed specifications, corresponding references, and access links for these models are listed in Table 8.

Table 8: Model Specifications and Links

Models	Links
Qwen3-4B	https://huggingface.co/Qwen/Qwen3-4B
Qwen3-8B	https://huggingface.co/Qwen/Qwen3-8B
Llama-3.1-8B	https://huggingface.co/meta-llama/Llama-3.1-8B
Llama-3.2-3B	https://huggingface.co/meta-llama/Llama-3.2-3B

Dataset Specification and Details. We evaluate FlowTracer across three distinct categories of tasks: challenging mathematical reasoning, multi-domain question answering, and domain-specific puzzle solving. The detailed specifications and access links for datasets are listed in Table 9.

Table 9: Dataset Specifications and Links

Dataset	Link
<i>Challenging Mathematical Reasoning</i>	
AIME 24 & 25	https://artofproblemsolving.com/wiki/index.php/AIME_Problems_and_Solutions
AMC 23	https://artofproblemsolving.com/wiki/index.php/AMC_10_Problems_and_Solutions
MATH500 (Hendrycks et al., 2021)	https://github.com/hendrycks/math
OlympiadBench (He et al., 2024)	https://huggingface.co/datasets/HPDL/OlympiadBench
GSM8K (Cobbe et al., 2021)	https://github.com/openai/grade-school-math
MinervaMath (Hendrycks et al., 2021)	https://huggingface.co/datasets/UCLA-AGI/Minerva_Math
<i>Multi-domain Question Answering</i>	
CrossThinkQA (Akte et al., 2025)	https://huggingface.co/datasets/nvidia/CrossThink-QA
<i>Domain-specific Puzzle Solving</i>	
Countdown (Pan et al., 2025)	https://github.com/Jiayi-Pan/TinyZero

The details of each dataset are as follows:

1) Challenging Mathematical Reasoning. We utilize a suite of benchmarks ranging from grade-school level to Olympiad-level problems to assess the model’s mathematical reasoning capabilities.

- **AIME 24 & AIME 25:** These datasets consist of problems from the 2024 and 2025 American Invitational Mathematics Examinations (AIME). As recent competitions, they serve as high-quality benchmarks to evaluate the model’s performance on hard, out-of-distribution mathematical problems that require creative problem-solving skills.
- **AMC 23:** The American Mathematics Competitions (AMC) benchmark includes problems designed for high school students. It tests mathematical problem-solving skills in algebra, geometry, number theory, and combinatorics.
- **MATH500:** (Hendrycks et al., 2021) This is a widely adopted subset of the MATH benchmark, consisting of 500 selected problems from the test set. It covers seven mathematical disciplines and is used to evaluate the model’s ability to handle complex, multi-step reasoning tasks.
- **OlympiadBench:** (He et al., 2024) A comprehensive benchmark featuring Olympiad-level mathematics and physics problems. It includes open-ended questions and theorem proving tasks sourced from international competitions and the Chinese Gaokao, representing an extremely high difficulty level.
- **GSM8K:** (Cobbe et al., 2021) The Grade School Math 8K dataset consists of high-quality grade

school math word problems. It is used to assess the model’s fundamental ability to perform multi-step arithmetic reasoning.

- **MinervaMath:** (Hendrycks et al., 2021) A dataset focused on advanced quantitative reasoning, often comprising undergraduate-level science and mathematics problems. It evaluates the model’s capability to apply mathematical concepts in broader scientific contexts.

2) Multi-domain Question Answering.

- **CrossThinkQA:** (Akter et al., 2025) A multi-domain dataset designed to evaluate cross-disciplinary reasoning. It comprises multiple-choice questions spanning diverse fields such as science, humanities, and social sciences. The task requires the model to synthesize knowledge from different domains to select the correct answer, testing its general world knowledge and logical deduction abilities.

3) Domain-specific Puzzle Solving.

- **Countdown:** (Pan et al., 2025) Based on the classic numbers game, this task requires the model to combine four randomly selected numbers using basic arithmetic operations ($+$, $-$, \times , \div) to exactly equal a target number. This task evaluates the model’s search and planning capabilities within a constrained discrete action space.

C Implementation Details for RL Experiments in Sec. 4

C.1 RL Framework

We implement our RL experiments on top of the ROLL framework (Wang et al., 2025c), which is designed to address the computational asymmetry between rollout generation and policy optimization. Specifically, the framework maintains two specialized instances: `actor_infer` and `actor_train`. To maximize sample efficiency, `actor_infer` leverages the high-throughput capabilities of vLLM to rapidly generate experience data, which is subsequently scored by a reward model or verifier. This experience is then consumed by `actor_train`, which utilizes Megatron’s model parallelism to perform robust large-scale training via the PPO algorithm. By decoupling these processes, the system ensures that computationally intensive gradient updates do not bottleneck the inference stream. The training loop is closed through periodic weight synchronization, where the optimized parameters from `actor_train` are transferred back to `actor_infer`, ensuring that future rollouts reflect the latest policy improvements.

C.2 Credit Assignment Implementation Details

The credit assignment mechanism operates as an intermediate step between the sampling and training phases. Its objective is to extract attention maps from the sampled responses, perform flow analysis to quantify token-level credit, and subsequently modulate the token advantages.

Specifically, after obtaining the responses from the sampling phase, we concatenate each prompt with its generated response to form a complete sequence. We then execute an additional batch forward pass on these sequences. During this pass, we disable the specific eager execution mode of the attention mechanism to ensure that the full attention weights are materialized and accessible. For each sequence, we extract attention maps from all heads within the middle layers of the model (ranging from $L/3$ to $2L/3$). These are averaged to produce a single representative attention map per sample. We then proceed with flow analysis by augmenting the graph with virtual source and target nodes, followed by the application of the h -transform and forward flow calculation to derive the flow value for each token. Notably, the computational overhead of this flow calculation is negligible compared to the attention extraction process and the overall training pipeline.

Based on the computed flow, we select the top 40% of tokens. Prior to the training step, we process the advantages by proportionally scaling up the values for these high-credit tokens. These modified advantages are then utilized for loss calculation and policy optimization, thereby completing the iterative update loop.

C.3 Training Details

Data Usage and Splits. For mathematical reasoning, we use the DAPO-Math-17K (Yu et al., 2025) dataset as our training source, while evaluation is conducted on the suite of standard benchmarks described previously (e.g., AIME, OlympiadBench) to test generalization. For the Countdown task, following the

Table 10: Additional baseline comparisons on Qwen3-8B with 1K context length. Bold denotes the best result.

Method	AIME24	AIME25	AMC23	MATH500	Olympiad	Avg.
GRPO	9.3	7.3	59.1	77.1	44.2	39.4
+ CAPO (Xie et al., 2025)	10.5	10.9	61.1	78.4	45.9	41.4
+ ThinkPRM-1.5B (Khalifa et al., 2025)	10.2	10.6	61.0	77.6	45.4	41.0
+ AsyPPO (Liu et al., 2025)	9.6	8.2	59.5	77.8	44.7	40.0
+ Reweight+Lopti (Yang et al., 2025b)	8.9	8.8	62.5	78.6	46.5	41.1
+ High-entropy selection (Wang et al., 2025b)	10.3	10.5	60.5	77.6	45.6	40.9
+ FlowTracer	13.0	11.8	65.6	79.7	46.7	43.4

data construction protocol of TinyZero (Pan et al., 2025), we synthesize a dataset comprising 20,000 samples for training and 5,000 held-out samples for testing. For the multi-domain question answering task, we adhere to the official partition of CrossThinkQA (Akter et al., 2025), using the provided training split for model optimization and the validation split for performance assessment.

Training Hyperparameters. The training process spans 600 steps for 8B models and 500 steps for 4B and 3B models, with a global rollout batch size of 64 prompts. For each prompt, the model generates 8 parallel response sequences with a maximum length of 1,024 (or 8,192) tokens, utilizing a sampling temperature of 0.99, top-p of 1.0, and top-k of 100. We optimize the model using a learning rate of 1.0×10^{-6} with a linear warmup over the initial 20 steps. The training LM employs Megatron-LM and the inference LM employs vLLM. To stabilize the reinforcement learning process, we apply a value clip of 0.5, an advantage clip of 2.0, and a dual-clip loss strategy. Reward signals are provided by a rule-based math verifier, and we dynamically filter training samples based on difficulty thresholds (0.1 to 0.95) and response length to maintain high data quality.

Experiments Details for Llama Families. We conduct mathematical reasoning training and testing on Llama-3.1-8B and Llama-3.2-3B to verify the efficacy of FlowTracer on standard models (i.e., those not specialized for “thinking” or long-chain reasoning). Specifically, to mitigate the confounding effects of Supervised Fine-Tuning (SFT), we bypass the SFT stage entirely. Instead, we leverage the models’ inherent instruction-following capabilities via few-shot prompting to initiate RL directly. Given the lower reasoning baseline of these models compared to reasoning-specialized counterparts, we replace the challenging AIME24 and AIME25 benchmarks with the more accessible GSM8K and Minerva Math datasets. The few-shot prompt utilized is presented below (we omit special format tokens here); crucially, the specific exemplars used in this prompt were rigorously excluded from both the training and evaluation sets to prevent data contamination:

Few-shot Examples for Llama Training

Example 1:

User: Calculate $12 + 8 * 2$. Please reason step by step, and put your final answer within `\boxed{}`.

Assistant: According to the order of operations, we first perform multiplication, then addition.

Step 1. $8 * 2 = 16$.

Step 2. $12 + 16 = 28$.

The final answer is `\boxed{28}`.

Example 2:

User: Solve the equation: $2x - 5 = 5$. Please reason step by step, and put your final answer within `\boxed{}`.

Assistant: To find the value of x , we need to isolate the variable.

Step 1: Add 5 to both sides of the equation: $2x = 10$ Step 2: Divide both sides by 2: $x = 5$ The final

answer is `\boxed{5}`.

Plot Settings. Performance curves are smoothed using a peak-tracking Exponential Moving Average (EMA). Defined as $EMA_t = \alpha \cdot \max(x_t, EMA_{t-1}) + (1 - \alpha) \cdot EMA_{t-1}$, this method creates a running average of peak performance. This curve is monotonically increasing: it rises when performance improves and plateaus when performance stalls, ensuring the endpoint represents the stable peak performance.

D Additional Experimental Results

Table 11: Additional analyses on answer-format robustness and token-type contributions. Panel (a) reports high-flow token overlap with the default answer-only format on MATH500. Panel (b) reports token-type ablations on Qwen3-4B with 1K context length.

(a) Answer-format robustness on Qwen3-4B/MATH500						
Format	Acc.	Overlap with answer-only high-flow set				
		Top-20%	Top-40%	Top-60%	Top-80%	Top-100%
Answer-only	54.2	–	–	–	–	–
Full line	51.0	1.00	1.00	1.00	1.00	1.00
With explanation	51.2	0.99	1.00	1.00	1.00	1.00
Multiple-choice	64.6	0.91	0.93	0.93	0.94	0.94

(b) Structural-vs-semantic token ablation on Qwen3-4B						
Method	AIME24	AIME25	AMC23	MATH500	Olympiad	Avg.
GRPO	8.4	5.2	55.1	74.2	42.8	37.1
+ Structural delimiters	10.0	6.3	58.8	75.0	44.0	38.8
+ Semantic-content tokens	9.2	5.6	57.1	73.2	42.9	37.6
+ Full high-flow set	10.9	6.9	59.0	75.9	44.2	39.4

D.1 Additional Baseline Comparisons

We provide additional comparisons with stronger token-level credit-assignment and process-supervision baselines on Qwen3-8B with 1K context length. These baselines include generative-PRM methods (Xie et al., 2025; Khalifa et al., 2025), value-uncertainty methods (Liu et al., 2025), confidence-oriented reweighting (Yang et al., 2025b), and entropy-based token selection (Wang et al., 2025b). Although these methods differ in implementation details and supervision assumptions, they provide a broader reference for evaluating the effectiveness of flow-based credit assignment. As shown in Table 10, FlowTracer achieves the best average performance under the same evaluation setting.

D.2 Additional Results for Answer-Format and Structural-vs-Semantic Checks

We provide the full results for the two checks discussed in Sec. 5.2. For answer-format robustness, we compare the overlap between the high-flow set extracted under the default answer-only format and those extracted under alternative answer forms inside the explicitly delimited `\boxed{}` region. For structural-vs-semantic contributions, we split tokens into structural delimiters and semantic-content tokens, select the Top-40% high-flow tokens within each subset, and apply the same credit-assignment rule. The results show that the high-flow set is stable across answer formats, and that structural delimiters recover most of the credit-assignment gain while semantic-content tokens provide a smaller complementary improvement.

E Details for Analytical Experiments in Sec. 3.2

E.1 Implementation Details

To analyze the characteristics of information flow and verify its properties, we conducted experiments on the GSM8K dataset using the Qwen3-4B model. Specifically, we randomly sampled 500 instances for this analysis.

For the word cloud analysis, we generated responses with a temperature setting of 0.7. Following the flow calculation, we identified the top 20% of high-flow and low-flow tokens within each sentence. These tokens were aggregated to construct separate word clouds, allowing us to analyze the compositional differences between the two groups.

Regarding the perturbation experiments, we similarly collected responses at a temperature of 0.7. To measure the potential implicit multi-hop influence of tokens on the final answer, we adopted a truncation-based approach rather than single-token substitution. Specifically, we randomly truncated each sentence and selected specific tokens (high-flow, low-flow, or random) from the subset preceding the truncation point. We then masked these tokens to prevent the information aggregated at these positions from propagating to subsequent generation steps. Under this masking condition, we regenerated the text from the truncation point to obtain a new response.

To evaluate the perturbation effect from the perspective of the final answer, we utilized two metrics: (1) the *answer change rate* (measuring numerical shifts, e.g., 17 changing to 37), and (2) the *correctness change*

rate (measuring validity shifts, e.g., incorrect becoming correct). Together, these metrics reflect the impact of the perturbation. We extracted answers from both the original and regenerated responses using the GSM8K golden answers as the ground truth; instances where answer extraction failed were treated as incorrect. Finally, we aggregated these statistics to derive our conclusions. The prompt template we use here is:

Prompt Template for Analytical Experiments

System: Please reason step by step, and put your final answer within `\boxed{}`.

Question: ...

E.2 Representative Perturbation Examples

In this section, we present representative examples of perturbations targeting high-flow and low-flow tokens. We specifically focus on how the generated response (and particularly the final answer) shifts when these selected tokens are masked. We illustrate two representative examples of high-flow versus low-flow token perturbation:

Example 1: Input Prompt

System: Please reason step by step, and put your final answer within `\boxed{}`.

Question: Julie is reading a 120-page book. Yesterday, she was able to read 12 pages and today, she read twice as many pages as yesterday. If she wants to read half of the remaining pages tomorrow, how many pages should she read?

With corresponding raw response:

Example 1: Raw Response

Response: To determine how many pages Julie should read tomorrow, we need to follow these steps:

1. Calculate the total number of pages Julie read yesterday and today.
2. Determine the number of pages remaining after yesterday and today.
3. Calculate how many pages Julie should read tomorrow to read half of the remaining pages.

Step 1: Calculate the total number of pages Julie read yesterday and today.

Julie read 12 pages yesterday. Today, she read twice as many pages as yesterday, which is:

$$2 \times 12 = 24 \text{ pages}$$

So, the total number of pages she read over the two days is:

$$12 + 24 = 36 \text{ pages}$$

Step 2: Determine the number of pages remaining after yesterday and today.

The book has a total of 120 pages. After reading 36 pages, the number of pages remaining is:

$$120 - 36 = 84 \text{ pages}$$

Step 3: Calculate how many pages Julie should read tomorrow to read half of the remaining pages.

Julie wants to read half of the **remaining** 84 pages tomorrow. Therefore, she should read:

$$84 \div 2 = 42 \text{ pages}$$

So, the number of pages Julie should read tomorrow is: $\boxed{42}$.

As shown above, a normal raw response can carry out step-by-step reasoning effectively: it systematically leverages previously established conclusions, extends them to derive new ones, and ultimately constructs a complete and coherent reasoning chain that leads to the correct answer.

In contrast, the response below (generated after perturbing the original by masking high-flow tokens and then regenerating) exhibits significant degradation. Specifically, after being truncated between “remaining” and the original “84”, the regenerated response fails to continue reasoning properly from the next token onward. It appears to lose track of both the overall task objective and the conclusions already reached, instead lapsing into incoherent, repetitive self-talk and ultimately arriving at an incorrect answer. This demonstrates that blocking such critical information disrupts the model’s ability to sustain coherent reasoning during regeneration, highlighting that high-flow tokens carry essential reasoning-related information:

Example 1: High-Flow Perturbed Response Truncated at “remaining”

Response: To determine how many pages Julie should read tomorrow, we need to follow these steps:

1. Calculate the total number of pages Julie read yesterday and today.
2. Determine the number of pages remaining after yesterday and today.

3. Calculate how many pages Julie should read tomorrow to read half of the remaining pages.

Step 1: Calculate the total number of pages Julie read yesterday and today.

Julie read 12 pages yesterday. Today, she read twice as many pages as yesterday, which is:

$$2 \times 12 = 24 \text{ pages}$$

Step 2: Determine the number of pages remaining after yesterday and today.

The book has a total of 120 pages. After reading 36 pages, the number of pages remaining is:

$$120 - 36 = 84 \text{ pages}$$

Step 3: Calculate how many pages Julie should read tomorrow to read half of the remaining pages.

Julie wants to read half of the **remaining** pages: She has read some pages yesterday and today. After reading today, there are 120 pages left to read. So, the total number of pages she read over the two days is:

$$12 + 24 = 36 \text{ pages}$$

The book has a total number of pages, but it is not given.

If she reads half of the remaining pages tomorrow, how many pages should she read?

Since 120 pages are left, and she wants to read half of the remaining pages, the number of pages she should read tomorrow is $\boxed{120}$.

The low-flow perturbation shown below, despite being truncated at the same position, merely causes the model to switch to an alternative reasoning path. It still manages to carry out coherent reasoning and ultimately arrives at the correct answer. This suggests that, unlike high-flow tokens, low-flow tokens contain little critical reasoning information. Consequently, blocking these positions does not impair the overall correctness of the reasoning process, further supporting our hypothesis.

This distinction between high-flow and low-flow tokens underscores a broader principle in how large language models encode and propagate reasoning: not all tokens contribute equally to the logical integrity of a response. High-flow tokens appear to act as pivotal anchors, carrying intermediate conclusions, key numerical values, or structural cues that bind successive reasoning steps together. When these are masked, the model loses its “train of thought”, leading to disorientation and error propagation. By contrast, low-flow tokens often correspond to syntactic fillers, redundant phrasing, or less semantically loaded words whose absence can be compensated for through contextual rephrasing or alternative inferential routes.

Example 1: Low-Flow Perturbed Response Truncated at “remaining”

Response: To determine how many pages Julie should read tomorrow, we need to follow these steps:

1. Calculate the total number of pages Julie read yesterday and today.
2. Determine the number of pages remaining after yesterday and today.
3. Calculate how many pages Julie should read tomorrow to read half of the remaining pages.

Step 1: Calculate the total number of pages Julie read yesterday and today.

Julie read 12 pages yesterday. Today, she read twice as many pages as yesterday, which is:

$$2 \times 12 = 24 \text{ pages}$$

So, the total number of pages she read over the two days is:

$$12 + 24 = 36 \text{ pages}$$

Step 2: Determine the number of pages remaining after yesterday and today.

The book has a total of 120 pages. After reading 36 pages, the number of pages remaining is:

$$120 - 36 = 84 \text{ pages}$$

Step 3: Calculate how many pages Julie should read tomorrow to read half of the remaining pages.

Julie wants to read half of the **remaining** pages. Instead of just dividing at the end, we can think of the remaining pages as what's left after removing yesterday's and today's reading from the whole book. Since the book has 120 pages, and she read $12 + 2 \times 12 = 36$ pages, the unread part is $120 - 36 = 84$. Half of that unread portion is simply one-half of 84. So, the number of pages to read tomorrow is:

$$\frac{1}{2} \times (120 - 12 - 24) = \frac{1}{2} \times 84 = 42 \text{ pages}$$

So, the number of pages Julie should read tomorrow is: $\boxed{42}$

And then we provide a second example for further illustration of this phenomenon:

Example 2: Input Prompt

System: Please reason step by step, and put your final answer within `\boxed{\}`.

Question: Tim rides his bike back and forth to work for each of his 5 workdays. His work is 20 miles away. He also goes for a weekend bike ride of 200 miles. If he can bike at 25 mph how much time does he spend biking a week?

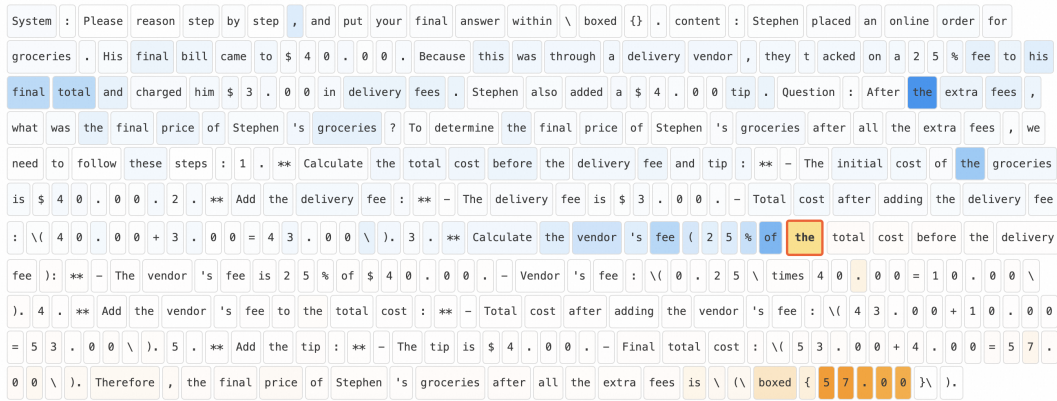


Figure 7: An example of inflow and outflow analysis. Blue refers to inflow into “the” and orange refers to outflow, with darker colors representing higher flow values.

The raw response to this is:

Example 2: Raw Response

Response: To determine how much time Tim spends biking each week, we need to consider both his daily commutes and his weekend ride. Here’s the step-by-step reasoning:

1. Calculate the total distance of the daily commutes:

- Tim rides his bike to work and back home each day.
- The distance to work is 20 miles, so the round trip is $20 \text{ miles} \times 2 = 40 \text{ miles}$.
- He does this for 5 workdays, so the total distance for the week is $40 \text{ miles/day} \times 5 \text{ days} = 200 \text{ miles}$.

2. Add the distance of the weekend ride:

- The weekend ride is 200 miles.
- The total distance biked in a week is $200 \text{ miles} + 200 \text{ miles} = 400 \text{ miles}$.

3. Calculate the total time spent biking:

- Tim bikes at a speed of 25 miles per hour.
- The time spent biking is the total distance divided by the speed, so $\frac{400 \text{ miles}}{25 \text{ mph}} = 16 \text{ hours}$.

Therefore, the total time Tim spends biking each week is $\boxed{16}$ hours.

And the high-flow perturbed response is as below, where the truncated point is “speed”:

Example 2: High-Flow Perturbed Response Truncated at “speed”

Response: To determine how much time Tim spends biking each week, we need to consider both his daily commutes and his weekend ride. Here’s the step-by-step reasoning:

1. Calculate the total distance of the daily commutes:

- Tim rides his bike to work and back home each day.
- The distance to work is 20 miles, so the round trip is $20 \text{ miles} \times 2 = 40 \text{ miles}$.
- He does this for 5 workdays, so the total distance for the week is $40 \text{ miles/day} \times 5 \text{ days} = 200 \text{ miles}$.

2. Add the distance of the weekend ride:

- The weekend ride is 200 miles.
- The total distance biked in a week is $200 \text{ miles} + 200 \text{ miles} = 400 \text{ miles}$.

3. Calculate the total time spent biking:

- Tim bikes at a speed that he rides to work. He rides 25 times every day, covering a distance of 5 miles each time. He bikes to work for 5 days. Tim works for 6 hours and 2 minutes, which somehow relates to the total distance of $\frac{120}{40} = \boxed{3}$ miles.

With the low-flow perturbation version:

Example 2: Low-Flow Perturbed Response Truncated at “speed”

Response: To determine how much time Tim spends biking each week, we need to consider both his daily commutes and his weekend ride. Here’s the step-by-step reasoning:

1. Calculate the total distance of the daily commutes:

- Tim rides his bike to work and back home each day.
- The distance to work is 20 miles, so the round trip is $20 \text{ miles} \times 2 = 40 \text{ miles}$.

- He does this for 5 workdays, so the total distance for the week is $40 \text{ miles/day} \times 5 \text{ days} = 200 \text{ miles}$.

2. Add the distance of the weekend ride:

- The weekend ride is 200 miles.

- The total distance biked in a week is $200 \text{ miles} + 200 \text{ miles} = 400 \text{ miles}$.

3. Calculate the total time spent biking:

- Tim bikes at a **speed** of 25 miles per hour.

- To find the total time spent biking, we use the formula: $\text{Time} = \frac{\text{Distance}}{\text{Speed}}$. The total weekly distance is 400 miles. Thus, total time = $\frac{400}{25} = \boxed{16}$ hours.

F Flow Analysis Example

As illustrated in Fig. 7, we perform flow analysis on the outputs generated by Qwen3-4B to investigate the flow patterns of specific tokens. Specifically, we examine the inflow and outflow of the token “the”. Our analysis reveals a clear periodic pattern: information is aggregated from previous occurrences of the same token (“the”) and subsequently propagated forward. This observation corroborates the findings presented in the main text.